A Kinetic Study of a Photo-Oxidation Reaction between α-Terpinene and Singlet Oxygen in a Novel Oscillatory Baffled Photo Reactor

Jianhan Chen , Rohen Prinsloo , Xiongwei Ni *

Posted Date: 15 December 2023

doi: 10.20944/preprints202312.1166.v1

Keywords: Photo-oxidation; singlet oxygen; reaction kinetics; reaction mechanism; oscillatory baffled photo reactor

Article

A Kinetic Study of a Photo-Oxidation Reaction between α-Terpinene and Singlet Oxygen in a Novel Oscillatory Baffled Photo Reactor

Jianhan Chen, Rohen Prinsloo and Xiong-Wei Ni *

Centre for Oscillatory Baffled Reactor Advancement, School of Engineering and Physical Sciences, Heriot-Watt University, Edinburgh EH14 4AS, UK

* Correspondence: x.ni@hw.ac.uk, tel:00441314513781

Abstract: By planting LEDs on the surfaces of orifice baffles, a novel batch oscillatory baffled photoreactor (OBPR) together with polymer-supported Rose Bengal (Ps-RB) beads are used to investigate reaction kinetics of a photo-oxidation reaction between α-terpinene and singlet oxygen ($^1O_2$). In the widely used NMR data analysis for this reaction, α-terpinene and ascaridole are treated as a reaction pair, assuming kinetically singlet oxygen is in excess or constant. We have, for the first time, examined the validity of the method, discovered that increasing α-terpinene initially leads to an increase of ascaridole, indicating that the supply of singlet oxygen is in excess. Applying kinetic analysis, a pseudo first order reaction kinetics is confirmed, supporting this assumption. We have subsequently initiated a methodology of estimating the $^1O_2$ concentrations based on the proportionality of ascaridole concentrations with respect to its maximum under these conditions. With the help of the estimated singlet oxygen data, the efficiency of $^1O_2$ utilization and the photo efficiency of converting molecular oxygen to $^1O_2$ are further proposed and evaluated. We have also identified conditions where further increase of α-terpinene has caused decreases in ascaridole, implying kinetically that $^1O_2$ has now become a limiting reagent, the method of treating α-terpinene and ascaridole as a reaction pair in the data analysis would no longer be valid under those conditions.

Keywords: photo-oxidation; singlet oxygen; reaction kinetics; reaction mechanism; oscillatory baffled photo reactor

1. Introduction

Heterogeneous photo-aided reactions and photocatalysis are initiated by the absorption of light. Scalable uniform mixing in handling multiphases and scalable uniform light distribution in providing light sources are two most critical requirements in photoreactors, so much so, the scalability of photoreactors has been identified as a key challenge in photochemical transformations in the chemical industry[1]. In terms of light provision, UV lamps/bars are traditionally placed outside or within reactors, suffering non-uniform distribution of light intensity, low power-to-photon efficiency and scale up ability[2]. LEDs, on the other hand, offer much narrower spectrum of light for targeted reactions and are sufficiently small to be installed within reactors, enabling uniform light distributions. LEDs have thus become the main light source in most of the lab scale photo reactors.

In terms of mixing, the century old problem remains where mixing gets worse with increasing scales: simply scaling up stirred tank reactors do not meet the above critical needs. Microreactors are seen as the viable alternative in solving the mixing issues, allowing safe exploitation of hazardous materials, while enabling optimal irradiance due to their narrow dimensions. Subsequently, a wide range of photochemistry applications using a variety of flow reactors have been reported in recent years[1, 3].

While lab-scale flow photoreactors are sufficient to produce small quantities of targeted molecules[4], applications in industrial scale photochemical processes are comparatively low due to

 doi:10.20944/preprints202312.1166.v1

the generally poor economics, complex scalability and safety issues of many photochemical transformations[5]. There are currently three main strategies in scaling up photo-microreactors: numbering up, lengthening the channel or increasing channel diameter[6]. Numbering up is a method of adding reactor systems in parallel until a desired productivity of chemicals is achieved. However, high inventory costs are a major drawback as multiple pumps, mass flow controllers and reactors are required[7]. Lengthening the flow path while keeping the channel diameter constant enables faster flow velocities while maintaining the same photon flux, but leads to issues with large pressure drops over the reactor[8]. Increasing diameter is the least viable method in scaling up microchannel reactors, as it weakens/diminishes diffusion-driven mixing in the reactor[9], providing poorer scale up than the former methods.

In this study, we present a novel batch Oscillatory Baffled Photo Reactor (OBPR) that provides uniform mixing and solid suspension via the succession and cession of eddies. Orifice baffles are one of the key intrinsic elements of the reactor set up, planting LEDs on the surfaces of orifice baffles[10] delivers uniform and controllable light distribution/intensity. The scale up of this device is through continuous oscillatory baffled reactors (COBR) that have a number of unique offerings: a) plug flow mixing is generated in laminar flows, minimizing pressure drop and allowing longer residence times[11]; b) uniform mixing is scalable[12]; c) COBR is good in handling solids[13] and have been implemented in industrial applications[14], meeting both critical requirements in photoreactors. The work to be presented in this paper is only associated with the batch OBPR. Using a model photo-oxidation reaction between α-terpinene and singlet oxygen ($^1O_2$), we report our kinetic analysis and assessment of the reaction. Polymer-supported rose Bengal beads are used in the work, because the OBPR has the excellent capability of suspending solids and enabling uniform light absorption.

2. The reaction scheme and experimental set up

2.1. Reaction scheme

The photo oxidation reaction is shown in Scheme 1 with polymer-supported Rose Bengal (Ps-RB) porous beads as the heterogeneous photosensitizer. The beads were synthesised in house and characterised according to known literature methods[15]. The first step of the reaction is that the photo absorption (+hν) by the Ps-RB chromophore promotes an electron to a higher-order singlet electronic excited state (^{1}[Ps-RB]*); ^{1}[Ps-RB]* converts to a triplet excited state (^{3}[Ps-RB]*) *via* intersystem crossing (ISC), which is the 2nd step; the energy transfer (EnT) from ^{3}[Ps-RB]* to ground state triplet molecular oxygen ($^3O_2$) occurs then *via* triplet-triplet annihilation (TTA), to return Ps-RB to its initial ground state and produces $^1O_2$; the next step is that $^1O_2$ spontaneously decomposes to $^3O_2$ *via* non-radiative decay (NRD) through vibronic energy transfer with solvent molecules, $^1O_2$ encounters α-terpinene in solution and undergoes a productive [4 + 2] cycloaddition to yield the endoperoxide product, ascaridole, known as a Diels-Alder-type reaction (Scheme 1). 1,3-Dienes commonly undergo [4+2] cycloaddition reactions with singlet oxygen $^1O_2$ to yield endoperoxides. This reaction has been extensively studied on naphthalene derivatives[16]. Other chemical transformations such as [2+2] additions or 'ene' type reactions are also possible, forming dioxetanes and hydroperoxides, respectively[17]. $^1O_2$ exists as a gas, but is dissolved in the reaction mixture or solvent[18]. Singlet oxygen is unstable, and its lifetime changes dramatically in different solvents, ranging from 4 to 628 μs[19], depending on the energy-transfer efficiency from electronic to intramolecular vibrational states, for instance, the lifetime in water is one order of magnitude lower than that in deuterated water. Chloroform ($CHCl_3$) provides the longest $^1O_2$ lifetime (~90 μs) of all common, non-deuterated laboratory solvents[20], hence was chosen as the solvent in this study. It should be noted that the amount of ascaridole produced does not equal to the amount of $^1O_2$ formed due to the non-radiative decay, but what is sure is that the formation of ascaridole is the direct evidence of the existence of singlet oxygen[2a].

Preprints (www.preprints.org) | NOT PEER-REVIEWED | Posted: 15 December 2023 doi:10.20944/preprints202312.1166.v1

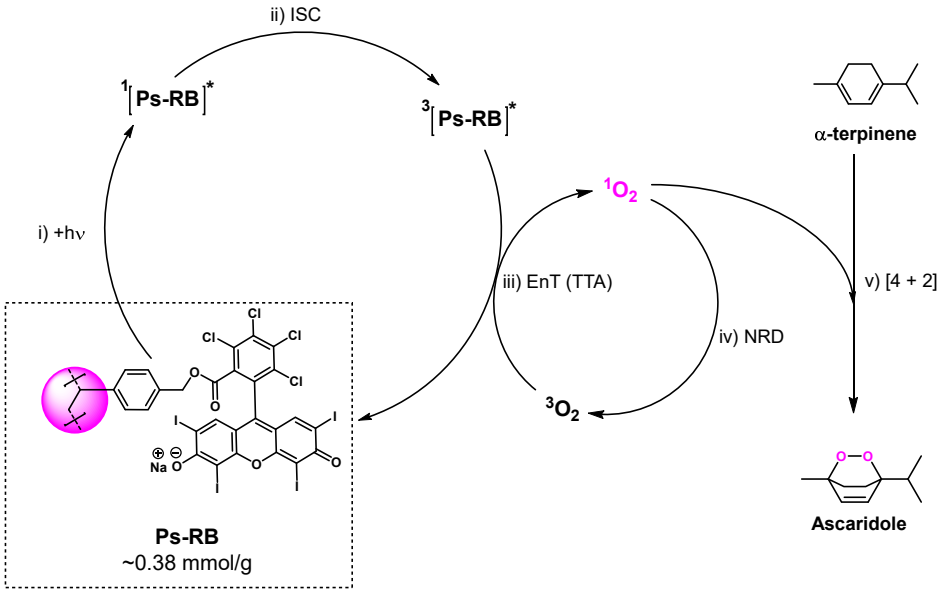

Scheme 1. Reaction scheme of singlet oxygen ($^1O_2$) photosensitisation by polymer-supported rose bengal (Ps-RB) and subsequent photooxidation of α-terpinene to produce ascaridole. (**Courtesy of Christopher Thomson**).

Heterogeneous photosensitizers have many advantages over homogeneous counterpart, for example, they are readily prepared, are easily removed post-reaction, when suspended in solution, do not accumulate or clog reactors. Heterogeneous photosensitizers are generally comprised of organic dyes bearing a (hetero)aromatic core, e.g. Rose Bengal (RB). Because RB suffers from extensive photobleaching/degradation under prolonged irradiation, the leakage is usually difficult to be removed from reaction effluents[21], modifications in synthesis have led to various robust solid photosensitizers. Previously, a versatile organic dye, 4,4-difluoro-4-bora-3a,4a-diaza-s-indacene (BODIPY), with a polymer-support was used as the photosensitizer in the same reaction, where BODIPY has nitrogen and boron containing heterocycles[4] with high fluorescence quantum yields and significant visible-light absorption, the ideal light wavelength fell between 500 and 540 nm. In this work, polymer-supported Rose Bengal (Ps-RB) porous beads are used, have high absorption coefficients in the visible spectral region and are stable after photosensitization, its optimal light wavelength is 530 nm[22]. The key advantage of Ps-RB over BODIPY is that the maximum absorbance wavelength is red-shifted and lower in energy, reducing the likelihood of photodecomposition of reactants and products[23].

2.2. Materials

α-terpinene was purchased from the Division of Tokyo Chemical Industry (TCI) (>90% purity), all organic solvents and reagents were sourced from Fisher Scientific at SLR grade, were used as received without further purification unless otherwise stated.

2.3. Reactor setup

The OBPR consists of a glass column of 50 mm in diameter and 480 mm in height as shown in Figure 1. The volume of the reactor is 600 ml, with the working volume of 500 ml. Orifice baffles have an outer dimeter of 46 mm, a hole diameter of 26 mm and a baffle spacing of 60 mm. Each set comprises of three orifice baffles, each baffle has 6 evenly spaced green LEDs (Cree 5-mm Round LEDs) planted on the lower surface (can also be both sides), as shown in Figure 1, for the purpose of providing light. The leads of LEDs are covered by epoxy resin that provides the insulation, material compatibility and corrosion resistance. The wavelength and light intensity of the green LEDs are 530 nm and 0.756 watts respectively. An air sparger is located at the base of the OBPR for introducing air at a controlled rate.

Preprints (www.preprints.org) | NOT PEER-REVIEWED | Posted: 15 December 2023 doi:10.20944/preprints202312.1166.v1

Based on a previous work in a microchannel reactor[6, 7b], about 390 mL $CHCl_3$ was mixed with 4.225 mL of α-terpinene in the OBPR in the presence of Ps-RB beads of 1600 mg. A constant liquid volume of 400 mL was maintained for all experiments. Oscillation frequency and amplitude were switched on once all chemicals were charged into the OBPR, the reaction was initiated when LEDs were turned on, the duration of the reaction was 120 mins. Runs were repeated for the data repeatability and reliability (see Table 1), averaged values were used in data presentation later.

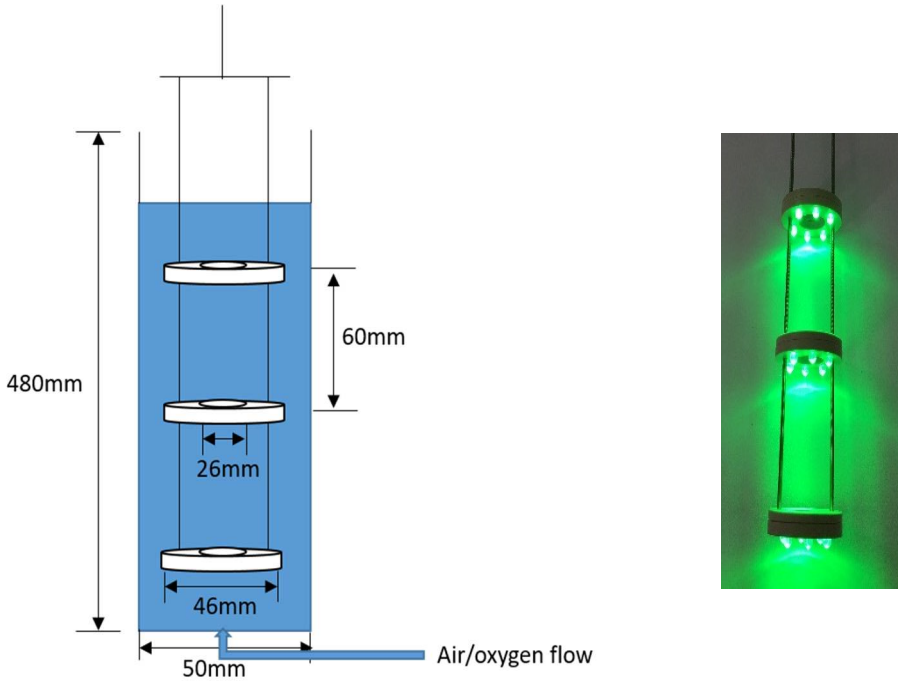

Figure 1. The schematic of OBPR reactor and orifice baffles with LEDs.

Table 1. Experimental conditions (bead mass = 1600 mg, irradiation wavelength = 530 nm, oscillation frequency = 2.5 Hz, oscillation amplitude = 24 mm, air flow rate = 172.5 ml/min, duration = 120 mins).

Run number	Chloroform (mL)	α-terpinene (mL)	Number of repeated runs
1	397.88	2.12	1
2	395.77	4.23 (default)	2
3	393.00	7.00	2
4	391.53	8.47	3
5	390.00	10.00	2
6	383.10	16.90	2
7	374.50	25.50	3

2.4. Analytic method

Samples were taken regularly and analysed using proton nuclear magnetic resonance (^{1}H NMR) to determine the composition/concentration of the mixture. The procedure of treating samples was performed as follows:

Preprints (www.preprints.org) | NOT PEER-REVIEWED | Posted: 15 December 2023 doi:10.20944/preprints202312.1166.v1

- Each 2 mL sample containing $CHCl_3$ + α-terpinene + ascaridole was injected to a dark vial to stop the reaction (reaction stops when light is off)
- The sample was placed into a round bottom flask and the solvent ($CHCl_3$) removed under reduced pressure on a rotary evaporator (40°C, 365 mbar for ~5 minutes)
- The oily residue was dissolved in 0.5 mL of deuterated chloroform ($CDCl_3$) and a ^1H NMR was obtained (300 MHz Bruker AVIII spectrometer)
- Peaks in the region between 6.70 and 5.40 ppm were used to determine the conversion of α-terpinene and the appearance of ascaridole

Figure 2 is a typical ^1H NMR spectra in chloroform-*d*, showing the alkenyl proton resonances of α-terpinene as a multiplet at 5.61 ppm, and ascaridole as a doublet-of-doublets centered at 6.45 ppm, consistent with previous reports[24], the resonance signals count for two alkenyl protons of the respective molecules. While p-cymene is a byproduct in the reaction, it is not detected by the ^1H NMR, which is consistent as other studies[25]. At the reaction stochiometric ratio of 1:1, the integrals of these signals are directly proportional to the relative concentrations of the two species. The concentration of α-terpinene at time t ($C_{\alpha T}$) is the ratio of the integrated NMR area of α-terpinene at time t ($Area_{\alpha T}$) over its corresponding area at time t=0 (taking as 100), multiplied by its initial concentration at t = 0 ($C_{\alpha T0}$ = 0.051917 mol/L). The concentration of ascaridole (C_{As}) is then the ratio of the integrated area of ascaridole over the total area at time t multiplied by the initial concentration of α-terpinene, since the initial concentration of ascaridole at t = 0 is zero as:

$$C_{\alpha T} = \left(\frac{Area_{\alpha T}}{Area_{\alpha T0}}\right) C_{\alpha T0} \quad C_{As} = \left(\frac{Area_{As}}{Area_{As}+Area_{\alpha T}}\right) C_{\alpha T0} \tag{1}$$

Since the byproduct is not detectable, $Area_{As}$ + $Area_{\alpha T}$ = 100, making the concentration of ascaridole a reaction pair of that of α-terpinene.

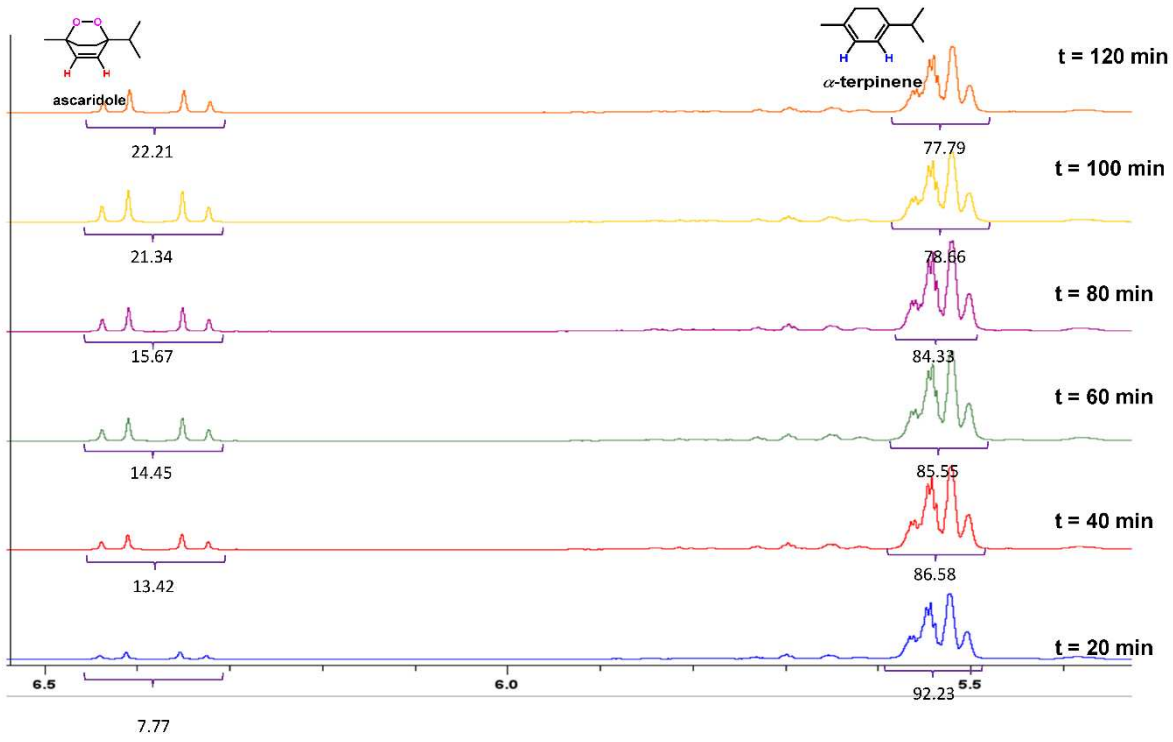

Figure 2. Stacked ^1H NMR spectra for monitoring the conversion of the two alkenyl protons of α-terpinene to ascaridole at an interval of 20 mins in the OBPR. Photo-oxidation conditions: mass of Ps-RB = 800 mg, irradiation wavelength = 530 nm, oscillation frequency = 2.5 Hz, oscillation amplitude = 24 mm, air flow rate = 172.5 ml/min.

3. Results and discussion

Preprints (www.preprints.org) | NOT PEER-REVIEWED | Posted: 15 December 2023 doi:10.20944/preprints202312.1166.v1

3.1. Kinetic assessment

The overall reaction in Scheme 1 can be described by a sequence of two reactions:

$$\text{oxygen} \underset{k2}{\overset{k1}{\rightleftharpoons}} \text{singlet oxygen}$$

$$\text{-Terpinene} + {}^{\lozenge}{}_{\kappa} \xrightarrow{k3} \text{ascaridole} \qquad (2)$$

Following the reaction scheme 1, some singlet oxygen ($^1O_2$) decomposes to molecular oxygen ($^3O_2$) *via* non-radiative decay (NRD), the first part of the reversible reaction counts for this process. At a fixed oscillatory frequency (f) and amplitude (x_0) in the OBPR with a known quantity of polymer-supported Rose Bengal beads at continuous controlled light irradiation at steady state, a net amount of $^1O_2$ (resulting from the 1st part of the reaction) is generated and reacts with α-terpinene to produce ascaridole (the 2nd part of the reaction). For one equivalent each of ascaridole and α-terpinene without any byproduct, the data analysis makes the consumption of α-terpinene as a reaction pair of the generation of ascaridole. This effectively assumes that the concentration of singlet oxygen is kinetically either in excess or constant. To the authors knowledge, no research publications have looked into this matter. In order to testify and verify this assumption, a number of planned experiments were carried out using different amounts of α-terpinene and chloroform while keeping the same reaction volume, see Table 1. Note that Run 2 was the default condition, based on previous studies.[4, 26]

Figure 3 compares the concentration profiles of ascaridole with different amounts of α-terpinene, an increase of the concentration of ascaridole as a function of time can be seen with the increase of α-terpinene in Figure 3a on the left (the filled symbols), this indicates that $^1O_2$ supply in the OBPR is indeed in excess. Further increases in the reagent however have brought decreases in the product (see the open symbols) in Figure 3b on the right, implying that under these experimental conditions, $^1O_2$ has become the limiting reagent, the concentration of ascaridole would solely be dependent upon the concentration of $^1O_2$, instead of α-terpinene, this stipulates that the widely used method of treating α-terpinene and ascaridole as a reaction pair in eq. (1) would no longer be valid under these conditions. Noted that chloroform is the solvent that does not participate in the reaction and is in significant excess over α-terpinene, its effect on the concentration of ascaridole should be of minimum, while not tested.

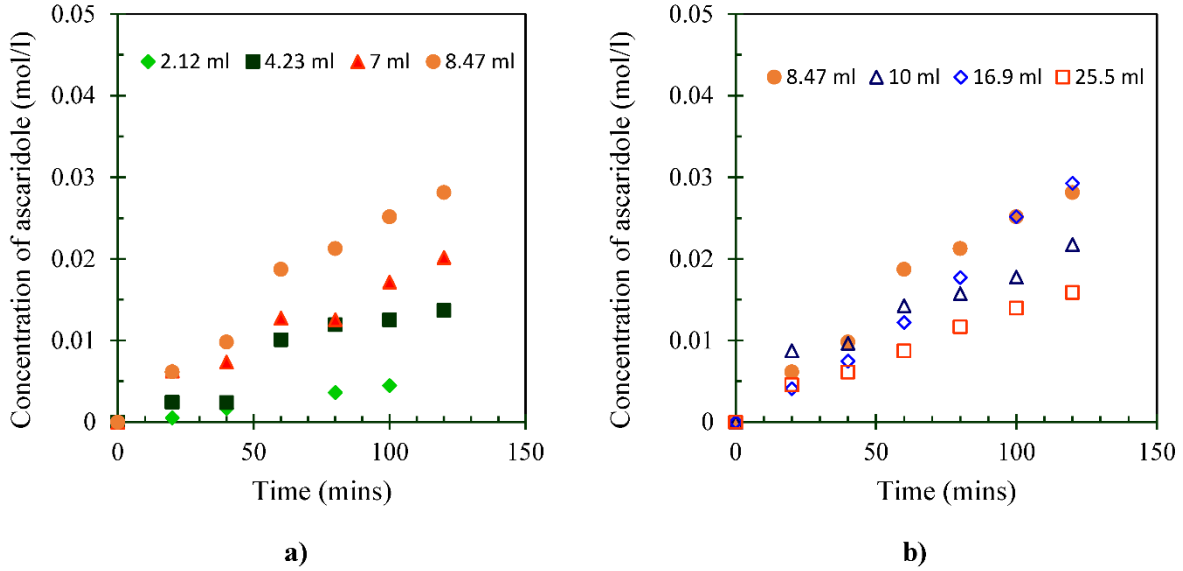

Figure 3. Concentration of ascaridole for different volumes of α-terpinene (bead mass = 1600 mg, irradiation

Preprints (www.preprints.org) | NOT PEER-REVIEWED | Posted: 15 December 2023 doi:10.20944/preprints202312.1166.v1

wavelength = 530 nm, oscillation frequency = 2.5 Hz, oscillation amplitude = 24 mm, air flow rate = 172.5 ml/min, duration = 120 mins).

Under the conditions where $^1O_2$ is in excess (Figure 3a), the 2nd order reaction of $^1O_2$ + α-terpinene $\xrightarrow{k3}$ ascaridole is then reduced to a pseudo first order of α-terpinene $\xrightarrow{k_3}$ ascaridole, it is then justified to treat the two as a reaction pair. The rate equation and the integral form are given below:

$$-\frac{dC_{\alpha T}}{dt} = k_3 C_{\alpha T} \qquad \ln\left(\frac{C_{\alpha T0}}{C_{\alpha T}}\right) = k_3 t \tag{3}$$

By plotting $\ln\left(\frac{C_{\alpha T0}}{C_{\alpha T}}\right)$ vs time for α-terpinene for 2.12, 4.23 and 7 ml, approximate straight lines can be seen in Figure 4, verifying the pseudo first order kinetics with the averaged rate constant of 0.0020 /min.

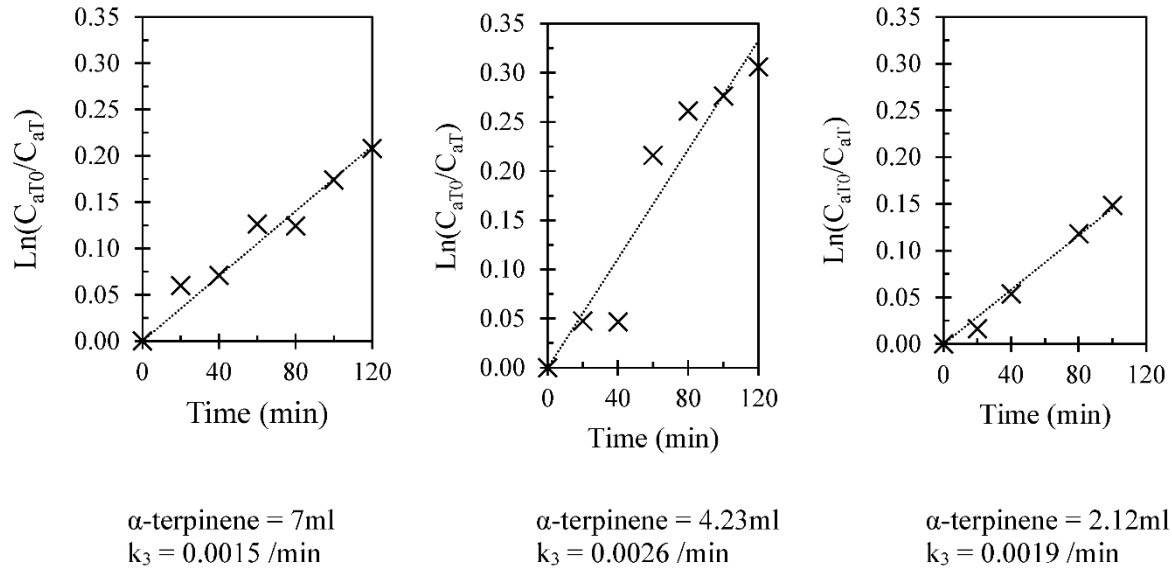

Figure 4. Fitting for pseudo first order kinetics (bead mass = 1600 mg, irradiation wavelength = 530 nm, oscillation frequency = 2.5 Hz, oscillation amplitude = 24 mm, air flow rate = 172.5 ml/min, duration = 120 mins).

At the 8.5 ml of α-terpinene, the conversion of ascaridole has reached the maximum, implying that neither singlet oxygen nor α-terpinene is in excess. Using the proportionality of ascaridole with respect to its maximum at 8.5 ml in Figure 3a, the excess $^1O_2$ concentrations for 7/4.23/2.12 ml of α-terpinene can be estimated using the equation below taking 7 ml as an example:

$$C_{O_2^1} = \left[1 + \frac{(C_{As})_{8.47ml} - (C_{As})_{7ml}}{(C_{As})_{8.47ml}}\right] \times C_{\alpha T} \tag{4}$$

Figure 5 shows the concentrations of all species for three volumes of α-terpinene. Note that there is no data of $^1O_2$ at t = 0, this is due to the concentration of ascaridole being zero at the start, $^1O_2$ concentrations were estimated from 20 mins onwards. We see that the concentrations of singlet oxygen are greater than that of α-terpinene, demonstrating that $^1O_2$ is in excess under those conditions. We also note that the concentration of $^1O_2$ is more or less unchanged at each amount of α-terpinene, this is consistent with what we stated earlier that a net amount of $^1O_2$ is generated in the OBPR at steady state.

Preprints (www.preprints.org) | NOT PEER-REVIEWED | Posted: 15 December 2023 doi:10.20944/preprints202312.1166.v1

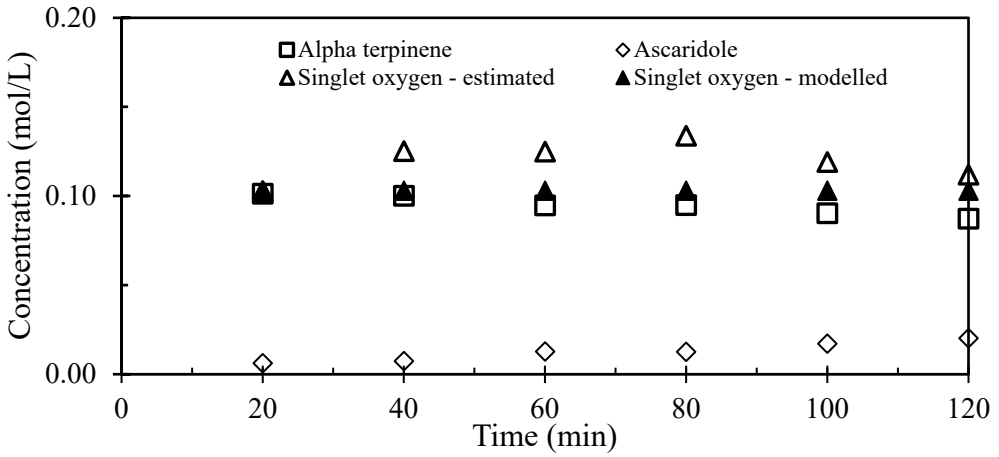

A) α-terpinene = 7 ml

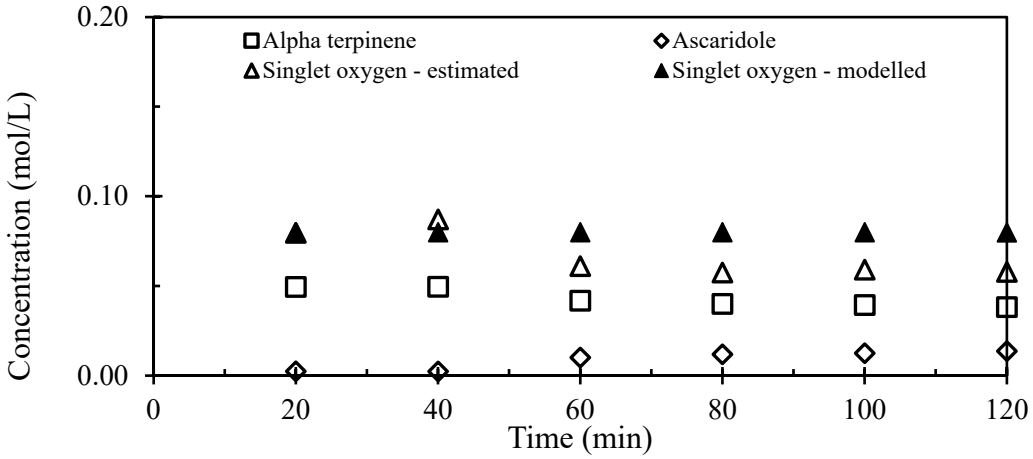

B) α-terpinene = 4.23 ml

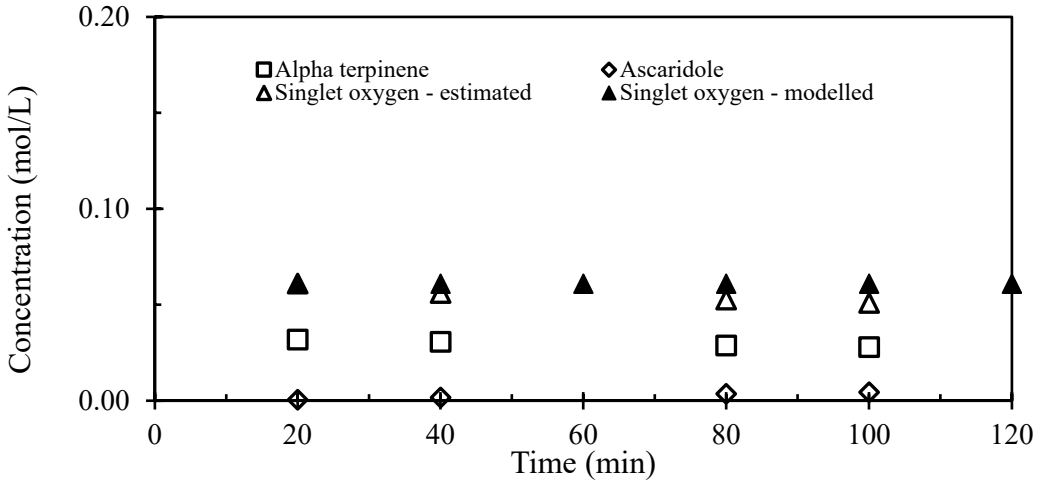

C) α-terpinene = 2.12 ml

Figure 5. Estimated singlet oxygen concentrations (bead mass = 1600 mg, irradiation wavelength = 530 nm, oscillation frequency = 2.5 Hz, oscillation amplitude = 24 mm, air flow rate = 172.5 ml/min).

Preprints (www.preprints.org) | NOT PEER-REVIEWED | Posted: 15 December 2023 doi:10.20944/preprints202312.1166.v1

By feeding the data of α-terpinene, ascaridole and k_3 (from Figure 4) into the reaction kinetic model in COPASI (Complex Pathway Simulator), the concentrations of singlet oxygen can be reconstructed as shown in Figure 5 (filled symbol). Note that COPASI is a versatile modelling tool that can be used for model development, model simulations (such as stochastic simulations and differential equation simulations), numerous sorts of analysis (such as sensitivity analysis, parameter estimation, and metabolic control analysis) as well as kinetic extraction.[27] We see that the estimated $^1O_2$ concentrations using the proportionality of ascaridole at different amounts of α-terpinene (open triangles) match reasonably well with these determined using the kinetic model (filled triangles). This further validates our proposed methodologies. We note that zero order reaction kinetics were reported by other studies for this reaction [25, 28], the zeroth order kinetics indicate that the reaction rate is a sole function of the reaction rate constant, does not depend on the concentrations of reagents. When we vary the concentrations of α-terpinene, the dependence of the reaction rate on the concentrations of the reagent is clearly demonstrated in our work.

Thanks to the estimated $^1O_2$ data, we can also evaluate the efficiency of $^1O_2$ utilization using the definition below, even when it is in excess as:

$$Efficiency\ of\ singlet\ oxygen\ utilization\ (\%) = 100\% - \frac{Singlet\ oxygen - ascaridole}{Singlet\ oxygen} \quad (5)$$

The efficiencies of $^1O_2$ utilization are tabulated in Table 2 for α-terpinene from 2.12 to 7 ml.

Table 2. Average efficiency of $^1O_2$ utilization and efficiency of photo conversion for three volumes of α-terpinene (photosensitizer = 1600 mg, irradiation wavelength = 530 nm, f = 2.5 Hz, x_0 = 24 mm, air flow = 172.5 ml/min, duration = 120 mins).

α-terpinene (ml)	Efficiency of $^1O_2$ utilization (%)	Efficiency of photo conversion (%)
7	10.7	0.10
4.23	14.6	0.07
2.12	4.9	0.06

3.2. The 1st step of the reaction

The process from molecular oxygen to $^1O_2$ in the first part of the overall reaction in eq. (2) relies on photo elevation/energy transfer. Due to a significant energy barrier (94 kJ/mol), $^3O_2$ molecules cannot directly be excited to $^1O_2$ due to it being a forbidden electronic transition by spin selection rules, and therefore requires a triplet photosensitiser to enable the triplet-triplet annihilation energy transfer mechanism[29]. When photons of the correct wavelength (<600 nm) irradiate the Ps-RB beads, the supported Rose Bengal chromophore is electronically excited and converts to a triplet-state *via* intersystem crossing (ISC), which enables it to undergo an energy transfer, resulting in the triplet-triplet annihilation process with oxygen to produce singlet oxygen[30]. The very short lifetime of singlet oxygen depends on temperature and solvent environment as vibronic energy transfer with solvent is a competitive, non-productive process which returns $^1O_2$ to its ground state, $^3O_2$ [31], referring to the 1st part of the overall reaction. Does the molecule oxygen refer to oxygen gas molecule[32] or dissolved oxygen? Air/oxygen is generally sparged into the reactor, of which a significant amount of gas bubbles exits the reactor without participating in the reaction, due to the density difference, the buoyance effect and critically the lack of mixing mechanism of holding bubbles within traditional reactors. This alludes that $^3O_2$ is associated with the dissolved oxygen. The process of converting oxygen gas to dissolved oxygen in chloroform is a mass transfer-controlled process, is mainly affected by mixing, air flow rate together with novel reactor designs. The properties of mixing in the OBPR are governed by the oscillatory Reynolds number[11c] (Re_o) and Strouhal number (St), defined as:

Preprints (www.preprints.org) | NOT PEER-REVIEWED | Posted: 15 December 2023 doi:10.20944/preprints202312.1166.v1

$$Re_0 = \frac{2\pi f x_0 \rho D}{\mu} \qquad St = \frac{D}{4\pi x_0} \tag{6}$$

Where D is the tube diameter (m), ϱ the fluid density (kg m^{-3}), x_0 the centre-to-peak amplitude (m), μ the viscosity (Pa s) and f the oscillatory frequency (Hz). The oscillatory Reynolds number is related to the intensity of mixing, the Strouhal number indicates the degree of eddy propagation.[11c, 13b] The effects of mixing (oscillation amplitude or *St*) and air flow rates on the conversion of ascaridole are given in Figure 6.

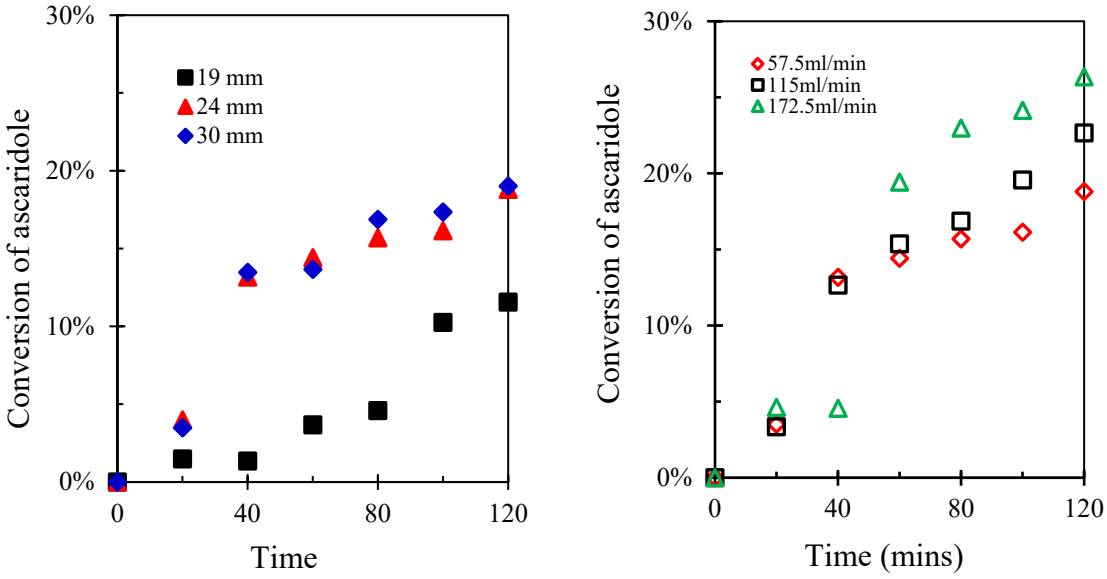

(A) air flow rate = 57.5 ml/min **(B)**

Figure 6. Conversion of ascaridole for different oscillation amplitudes (A) and air flow rates (B) (bead mass = 1600 mg, irradiation wavelength = 530 nm, oscillation frequency = 2.5 Hz, oscillation amplitude = 24 mm).

We see that generally the higher the oscillation, the higher the conversion (Figure 6A). As mixing intensity increases in the OBPR, the intensive and uniform mixing breaks up bubbles, leading to a decrease in bubble sizes and increase in bubble surface area; these bubbles are trapped in the vortices for longer periods of time, enhancing residence time for mass transfer within the reactor,[33] the direct result is more dissolved oxygen concentration in the solvent[34] and more excited molecular oxygen, in turn more $^1O_2$*. The amount of improvement in conversion is however rather limited for all amplitudes. The effect of air flow rate on the conversion (Figure 6B) tells a similar story, the higher the air flow rate, the higher the conversion, but there is an operational limit for further increasing air flow rate, as channelling takes place, bringing out the beads from the OBPR. The highest flow rate was used in the experiments of kinetics studies.*

By comparing the total amount of air/oxygen sparged into the OBPR with the estimated amount of $^1O_2$ every 20 mins, the efficiency of photo conversion of $^1O_2$ can be evaluated as

$$Efficiency\ of\ photo\ conversion\ of\ singlet\ oxygen\ (\%) = 100\% - \frac{Oxygen\ input - Singlet\ oxygen}{Oxygen\ input} \tag{7}$$

The oxygen input is calculated using the air flow rate (21% oxygen) and the time duration, the $^1O_2$ concentration is then converted into mass for the same time duration. Table 2 summarizes both efficiencies.

The limited conversion to ascaridole in Figures 5 & 6 is the direct result of the combined low efficiency of $^1O_2$ utilization with very low efficiency of converting $^3O_2$ to $^1O_2$, the latter is perhaps the number 1 barrier for this reaction, indeed for most photo-aided reactions and photocatalysis. The low

 doi:10.20944/preprints202312.1166.v1

conversion to ascaridole is also consistent with previous work, albeit with BODIPY as the photosensitizer[35]. We are in the process of expanding this work to determine the pressure dependence of $^1O_2$ by varying the partial pressures.

Conclusions

Four brand new results are reported in this paper, firstly expanding on the success of continuous oscillatory baffled reactor technology, we have introduced a novel batch oscillatory baffled photoreactor (OBPR) with LEDs planted evenly on the surfaces of orifice plates, allowing uniform and controlled light distribution for photo-aided reactions and photocatalysis from lab to full scales; Secondly, using a model photo-oxidation reaction with solid photosensitizer, we have carried out a full examination of the validity of treating α-terpinene and ascaridole as a reaction pair in the widely used NMR data analysis. We unveiled that increasing α-terpinene initially leads to an increase of ascaridole, implying that the supply of singlet oxygen is in excess. Applying the pseudo first order reaction kinetics, the results fully support this hypothesis, validating the data analysis under these conditions. Further increases of α-terpinene however has led to decreases in ascaridole, implying kinetically that $^1O_2$ has become the limiting reagent, the method of treating α-terpinene and ascaridole as a reaction pair in the data analysis would no longer be valid under those conditions. Thirdly, we have initiated a method of estimating the concentrations of $^1O_2$ using the concentration profiles of ascaridole with respect to its maximum, $^1O_2$ in excess is demonstrated in each of the α-terpinene volumes. Knowing the concentrations of α-terpinene and ascaridole together with the rate constant, we have reconstructed the $^1O_2$ concentrations that match reasonably well with the estimated values. Lastly, with the estimated $^1O_2$ data, we proposed a methodology of evaluating the efficiency of $^1O_2$ utilization and the photo efficiency of converting $^3O_2$ to $^1O_2$. It is the combination of the above two deficiencies that has led to the overall low conversion of ascaridole (~20%) in this photo-oxidation.

Acknowledgements: Authors wish to express special thanks to Christopher Thomson and Dr Filipe Vilela, Institute of Chemistry Science, Heriot-Watt University for supplying photosensitizers, the associated information for synthesis and characterisation; Andrew Haston for fabricating the LED baffles and Douglas Wagener for constructing the experimental rigs.

Conflict of interest: Authors have no conflict interest for the work reported in this paper.

Nomenclature

$Area_{as}$	integrated NMR area of ascaridole
$Area_{\alpha T}$	integrated NMR area of α-Terpinene
C_{as}	concentration of ascaridole (mol L^{-1})
$C_{\alpha T}$	concentration of α-Terpinene (mol L^{-1})
D	tube diameter (m)
f	oscillation frequency (Hz)
Re_o	oscillatory Reynolds number
St	Strouhal number
x_o	oscillatory center-to-peak amplitude (m)
ρ	density (kg m^{-3})

References

1. L. Buglioni, F. Raymenants, A. Slattery, S. D. A. Zondag, T. Noël, *Chem Reviews* **2022**, *122*, 2752-2906.
2. aF. Ronzani, N. Costarramone, S. Blanc, A. K. Benabbou, M. L. Bechec, T. Pigot, M. Oelgemöller, S. Lacombe, *Journal of Catalysis* **2013**, *303*, 164-174; bM. S. Baptista, J. Cadet, P. D. Mascio, A. A. Ghogare, A. Greer, M. R. Hamblin, C. Lorente, S. C. Nunez, M. S. Ribeiro, A. H. Thomas, M. Vignoni, T. M. Yoshimura, **2017**, *93*, 912-919.
3. aS. D. A. Zondag, D. Mazzarella, T. Noël, *Annual Review of Chemical and Biomolecular Engineering* **2023**, *14*, 283-300; bE. Kayahan, M. Jacobs, L. Braeken, L. C. J. Thomassen, S. Kuhn, T. V. Gerven, M. Enis Leblebici, *Beilstein J. Org. Chem.* **2020**, *16*, 2484–2504; cA. Chaudhuri, K. P. L. Kuijpers, R. B. J. Hendrix, P. Shivaprasad, J. A. Hacking, E. A. C. Emanuelsson, T. Noël, J. V. D. Schaaf, *Chemical Engineering Journal* **2020**, *400*; dK.

Donnelly, M. Baumann, *J Flow Chem* **2021**, *11*, 223–241; eD. S. Lee, Z. Amara, C. A. Clark, Z. Xu, B. Kakimpa, H. P. Morvan, T. J. Pickering, M. Poliakoff, M. W. George, *Organic Process Research & Development* **2017**, *21*, 1042-1050.

4. J. M. Tobin, J. Liu, H. Hayes, M. Demleitner, D. Ellis, V. Arrighi, Z. Xu, F. Vilela, *Polymer Chemistry* **2016**, *7*, 6662-6670.
5. O. Shvydkiv, K. Jähnisch, N. Steinfeldt, A. Yavorskyy, M. Oelgemöller, *Catalysis Today* **2018**, *308*, 102-118.
6. Z. Dong, Z. Wen, F. Zhao, S. Kuhn, T. Noël, *Chemical Engineering Science: X* **2021**, *10*.
7. aY. Su, K. Kuijpers, V. Hessela, T. Noël, *Reaction Chemistry & Engineering* **2015**, *1*, 73-81; bK. P. L. Kuijpers, M. A. H. van Dijk, Q. G. Rumeur, V. Hessel, Y. Su, T. Noël, *Reaction Chemistry & Engineering* **2017**, *2*, 109-115.
8. E. G. Moschetta, S. M. Richter, S. J. Wittenberger, *ChemPhotoChem* **2017**, *1*, 539-543.
9. aG. I. Taylor, *Royal Society* **1954**, *225*, 473–477; bG. I. Taylor, *Royal Society* **1953**, *219*, 186-203.
10. X. Ni, in *WO2022013348A1*, **2022**.
11. aM. R. Mackley, X. Ni, **1991**, *46*, 3139-3151; bX. Ni, H. Jian, A. W. Fitch, *Chemical Engineering Science* **2001**, *57*, 2849-2862; cX. Ni, M. R. Mackley, A. P. Harvey, P. Stonestreet, M. H. I. Baird, N. V. Rama Rao, *Chemical Engineering Research and Design* **2003**, *81*, 373-383; dA. W. Dickens, M. R. Mackley, H. R. Williams, **1989**, *44*, 1471–1479.
12. aH. Jian, X. Ni, **2005**, *83* 1163-1170; bX. Ni, Y. S. Gélicourt, J. Neil, T. Howes, *Chemical Engineering Journal* **2002**, *85*, 17-25.
13. aG. Jimeno, Y. C. Lee, X. Ni, *The Canadian Journal of Chemical Engineering* **2021**, *100*, S258-S271; bM. Jiang, X. Ni, *Organic Process Research & Development* **2019**, *23*, 882-890.
14. NiTech.
15. aM. I. Burguete, F. Galindo, R. Gavara, S. V. Luis, M. Moreno, P. Thomas, D. A. Russell, **2008**, *8*, 37-44; bV. Fabregat., M. I. Burguete., F. Galindo., S. V. Luis., *Environmental Science and Pollution Research* **2013**, *21*, 11884–11892.
16. aJ. M. Aubry, B. Mandard-Cazin, M. Rougee, R. V. Bensasson, *Journal of the American Chemical Society* **1995** *117*, 9159-9164; bW. Adam, M. Prein, *Journal of the American Chemical Society* **1993**, *115*, 3766-3767; cM. Bauch, W. Fudickar, T. Linker, *Molecules* **2021**, *26*, 804.
17. A. A. Ghogare, G. Greer, *Chemical Reviews* **2016**, *116*, 9994-10034.
18. L. Villén, F. Manjón, D. García-Fresnadillo, G. Orellana, *Applied Catalysis B: Environmental* **2006**, *69*, 1-9.
19. M. A. J. Rodgers, *NATO ASI Series A, Vol. 85*, Life Sciences, **1984**.
20. P. R. Ogilby, C. S. Foote, *Journal of the American Chemical Society* **1983**, *105*, 3423-3430.
21. aE. Gianotti, B. M. Estevão, F. Cucinotta, N. Hioka, M. Rizzi, F. Renò, L. Marchese, *An Efficient Rose Bengal Based Nanoplatform for Photodynamic Therapy, Vol. 20*, Chemistry : a European journal, **2014**; bC. Whitmire, *Photosensitizers: Types, Uses and Selected Research*, Nova Science Publishers, **2016**.
22. M. S. Deshpande., V. B. Rale., J. M. Lynch., *Enzyme and Microbial Technology* **1992**, *14*, 514-527.
23. Y. L. Wong, J. M. Tobin, Z. Xua, F. Vilela, *Journal of Materials Chemistry A* **2016**, *4*, 18677-18686.
24. K. Zhang, D. Kopetzki, P. H. Seeberger, M. Antonietti, F. Vilela, *Angew Chem Int Ed Engl* **2013**, *52*, 1432-1436.
25. K. S. Elvira, R. C. R. Wootton, N. M. Reis, M. R. Mackley, A. J. deMello, *ACS Sustainable Chem. Eng* **2013**, *1*.
26. aJ. Shen, R. Roman Steinbach, J. Tobin, M. M. Nakata, M. Bower, M. R. S. McCoustra, H. Bridle, V. Arrighi, F. Vilela, *Applied Catalysis B: Environmental* **2016**, *193*, 226-233; bC. G. Thomson, C. M. S. Jones, G. Rosair, D. David Ellis, J. M. Hueso, A. L. Lee, F. Vilela, *Journal of Flow Chemistry* **2020**, *10*, 327-345.
27. S. Hoops, S. Sahle, R. Gauges, C. Lee, J. Pahle, N. Simus, M. Singhal, L. Xu, P. Mendes, U. Kummer, *Bioinformatics* **2006**, *22*, 3067-3074.
28. aS. Alofi, O'Rourke., C. Mills, *Photochem Photobiol Sci* **2022**, *21*; bV. L. Luke, L. V. , S. S. Rickenbach, T. M. McCormick, *Journal of Photochemistry and Photobiology A: Chemistry* **2019**, *378*, 131-135.
29. P. R. Erickson, K. J. Moor, J. J. Werner, D. E. Latch, W. A. Arnold, K. McNeill, *Environ Sci Technol* **2018**, *52*, 9170-9178.
30. R. M. Hockey, J. M. Nouri, *Chemical Engineering Science* **1996**, *51*, 4405-4421.
31. J. Zhao, W. Wu, J. Suna, S. Guo, *Chem. Soc. Rev.* **2013**, *42*, 5323-5351.
32. aW. R. Midden, S. Y. Wang, *American Chemical Society* **1983**, *105*, 13; bM. O. Sunday, H. Sakugawa, *Science of The Total Environment* **2020**, *746*.
33. M. S. N. Oliveira, X. Ni, *AIChE Journal* **2004**, *50*, 3019-3033.

34. S. M. R. Ahmed, A. N. Phan, A. P. Harvey, *Chemical Engineering & Technology* **2017**, *40*, 907-914.
35. C. G. Thomson, C. M. S. Jones, G. Rosair, D. Ellis, J. Marques-Hueso, A. L. Lee, F. Vilela, *Journal of Flow Chem* **2020**, *10*.